Lipid Nanotubes as an Organic Template for an Electrically-Conductive Gold Nanostructure Network

Kristina Jajcevic[1], Kaori Sugihara[2]*

[1]Department of Physical Chemistry, University of Geneva, Quai Ernest Ansermet 30, 1211 Geneva 4, Switzerland

[2]Institute of Industrial Science, The University of Tokyo, 4-6-1 Komaba Meguro-Ku, Tokyo 153-8505, Japan

ABSTRACT:

We demonstrate an approach to fabricate a gold nanowire network that presents a macroscopic electrical conductivity based on a lipid nanotube (LNT) template with attached gold nanoparticles. The poor electrical conductivity that we have previously faced was overcome by centrifugation and resuspension of gold nanoparticle solution for removing stabilizing agents, which increased the density of gold nanoparticles on the LNTs. An additional electroless metal plating further enhanced their contacts at nanoscale. Thanks to these procedures the sheet resistance was improved by 11 orders of magnitude. As a proof of principle, transparent conductive films were fabricated with these gold nanowires, which exhibited sheet resistance of maximum 70 Ω/□ and transmittance of 50-75% in visible light.

KEYWORDS: *lipid self-assembly, lipid nanotubes, organic template*

Table 1: Comparison of nanofabrication techniques[1-7]

	Feature size	Throughput	Equipment demand	Comments
Lithography				
UV lithography	> 10 nm	High	High	Dimension limits due to wavelength
Extreme UV lithography	< 10 nm	High	High	Difficult to fix defects
Electron beam lithography	< 10 nm	Low	High	Backscattering of electrons limits minimum spacing between pattern features
Focused ion beam lithography	< 10 nm	Low	High	Extensive substrate damage
Scanning probe lithography				
Scanning tunneling microscope lithography	10-50 nm	Low	High	Mostly used for mask repair
Atomic force microscope lithography	10-50 nm	Low	High	Mostly used for mask repair
Nanoimprint lithography	< 15 nm	High	Low*	Limited to soft lithography
Self-assembled templates				
Colloidal lithography	< 10 nm	High	Low	Limited to specific pattern
DNA self-assembly	< 5 nm	High	Low	It does not require expensive equipment but DNA (templating material) is expensive

* Relies on a mask aligner for fabricating the mold

INTRODUCTION

Nanostructured surfaces have broad applications such as photovoltaic devices,[8-9] next generation batteries,[10-12] sensors,[13-16] metamaterials,[17-20] wearable healthcare devices,[21-23] tissue engineering,[24] enzyme-coated[25] and anti-bacterial surfaces.[26-27] The emergence of these nanotechnologies is accompanied by the advancement of nanofabrication methods to shape, position, and organize objects at nanoscale to go beyond the conventional top-down lithography in terms of feature size, throughput or reduced required equipment for minimizing the cost (see the comparison in Table 1). Organic templating based on self-assembled biomolecules is one of the approaches that can potentially provide a higher throughput thanks to the self-assembly and lower prices because of the wet-chemistry-based processes without use of expensive machines. Magnolia liliiflora leaf veins have been previously exploited to fabricate conductive transparent substrates by electroless metal plating of copper.[28] Their performance in terms of the transparency in visible wavelength (86%) and the sheet resistance that is two orders of magnitude lower than that of ITO films is excellent, however, their feature size is relatively large (sub- to several micrometer) and the use of natural leaves hinder controlled large scale productions. Tobacco mosaic virus[29-32], DNA[33-39] and lipid nanotubes[40-

[41] have been also used as a template for metal plating to fabricate conductive nanoparticles dispersed either in solution or on substrates. Especially DNA is programmable, which has an advantage for creating nearly arbitrary shapes. However, such nanoparticles could not be connected into a macroscopic network efficiently because even the biggest DNA origami to date is in the range of sub-micrometer.[42-43] In addition, DNA is expensive as a templating material. This limits their application in electronics such as transparent conductive films, fractal electrodes, and electrochemical plasmonic sensors because a homogenous macroscopic conductivity is difficult to achieve with these substrates with dispersed conductive nanoparticles due to a poor and uncontrolled electrical connection between the particles. Therefore, the combination of the fabrication of nanosized objects and their assembly into a network over a macroscopic area based on organic templating remains as a challenge.

In this work, we demonstrate an approach to fabricate a gold nanowire network that presents a macroscopic electrical conductivity based on lipid nanotube (LNT) templates. LNTs employed in this work[44-49] have a diameter of around 20 nm, thus transferring their architecture to solid materials by wet chemistry enables fabrication of nanostructures without using expensive equipment. In addition, lipids are cheap and safe, while their amphiphilic nature allows material-efficient self-assembly with high throughput.[50-51] All these aspects make it an attractive candidate for nanofabrication templates. Gold nanoparticles (AuNP) were attached to these pre-patterned LNT templates via biotin-streptavidin binding for the alignment. Previously we have suffered from the poor electrical conductivity from these substrates due to the lack of connections between AuNPs.[44] In this work, we introduced electroless metal plating to dramatically improve the electrical conductivity of the aligned AuNPs. As a proof of principle, we fabricated transparent conductive films made of gold nanowires (AuNW) on glass substrates, which exhibited sheet resistance of maximum 70 Ω/□ and transmittance of 50-75% in visible light.

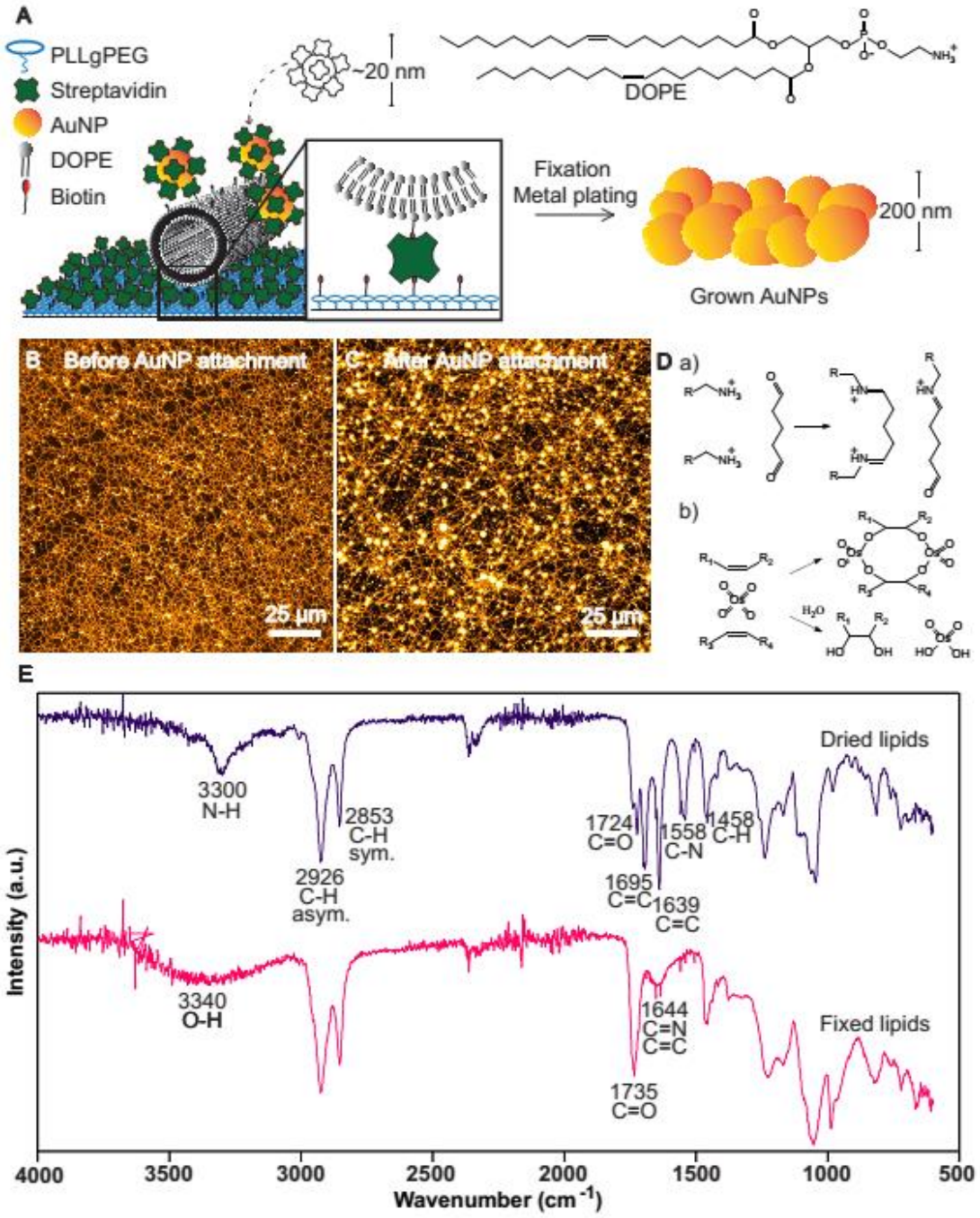

Figure 1: (A) Chemical structure of DOPE and a scheme describing the fabrication procedure of gold nanowires (AuNW) based on lipid nanotube templates. (B, C) Fluorescent images of self-assembled lipid nanotubes (LNT) before and after gold nanoparticle (AuNP) attachment, respectively. Note that the enhancement of these images is not equal, because the fluorescence intensity of LNTs from (C) is dimmer due to photobleaching that takes place during the AuNP attachment process. (D) The reaction mechanisms of chemical fixation of DOPE with (a) glutaraldehyde and (b) osmium tetraoxide. (E) Infrared spectra of dried and fixed lipids.

MATERIALS AND METHODS

Buffer Solution (HEPES): All the experiments were performed in HEPES buffer solution at pH 7.4. The buffer solution was prepared with 10 mM 4-(2-hydroxyethyl)piperazine-1-ethanesulfonic acid (Sigma Aldrich, Switzerland) and 0.15 M sodium chloride (Sigma Aldrich, Switzerland) in ultra-pure water filtered through MilliQ Gradient A10 filters (Millipore AG, Switzerland). The pH was adjusted to 7.4 using 6 M NaOH (Sigma Aldrich, Switzerland). It was sterile filtrated through 0.22 μm porous membranes before use.

Surface Functionalization with Polyelectrolytes: PLL-g-PEG and PLL-g-PEG-biotin (Polylysine (20 kDa) grafted with polyethyleneglycol (2 kDa), #PLL(20)-g[3.5]-PEG(2)) were purchased from SuSoS AG (Switzerland) and dissolved in ultrapure water at 0.1 mg mL^{-1}. For the PLL-g-PEG-biotin coating, an oxygen-plasma-treated glass coverslip was incubated in PLL-g-PEG/PLL-g-PEG-biotin solution (2:1) for 30 min and rinsed with ultrapure water. The mixture of biotin-tagged PLL-g-PEG and PLL-g-PEG permits to control the density of biotin on surfaces. The same method was used for the coating of silicon grids for transmission electron microscopy (TEM) and silicon wafers for scanning electron microscopy (SEM). After the functionalization of the surfaces, the substrates were incubated in streptavidin (#S4762, Sigma-Aldrich, Switzerland) solution (50 μg mL^{-1}) for 45 min and rinsed with ultrapure water.

Lipid Nanotube Assembly: The lipid solution were prepared as reported in our previous work[44]. 1,2-dioleoyl-sn-glycero-3-phosphoethanolamine (DOPE, #850725), 1,2-dioleoyl-*sn*-glycero-3-phosphoethanolamine-N-(cap biotinyl) (BiotinPE, #870273), and 1,2-dioleoyl-*sn*-glycero-3-phosphoethanolamine-N-(lissaminerhodamine B sulfonyl) (RhodaminePE, #810150) were purchased from Avanti Polar Lipids and stored in chloroform. The lipid solution was prepared by mixing 96% DOPE + 4% BiotinPE + 0.1% RhodaminePE in a flask, drying in vacuum for

minimum 2 h and adding HEPES buffer solution, followed by sonication at the final concentration of 1.0 mg mL^{-1}. Upon sonication, lipids detach from the flask wall and form blocks of H_{II} phase. The lipid blocks were adsorbed onto the substrates coated with PLL-g-PEG-biotin-streptavidin. The interaction between BiotinPE and the streptavidin exposed on the surface promotes the attachment of the lipids, while the PEG passivates the nonspecific adsorption. A turbulent flow was given by a pipette to create random LNT networks followed by rinse with HEPES buffer solution. To attach the AuNPs along the LNTs the created LNTs were incubated under streptavidin-AuNP solution (Cytodiagnostics, Canada, 5.96×10^{13} particles mL^{-1}) for 15 min, followed by rinse with HEPES buffer.

Sample Chambers: All samples were confined in sample chambers consisting of a donut-shaped polydimethylsiloxane (PDMS) block and a glass coverslip cleaned by an oxygen-plasma cleaner (TePla IoN 3Mz oxygen plasma machine, PVA TePla, Germany) just before the experiments. The PDMS blocks adhere to the glass surface and act as a wall to confine liquid inside.

Fluorescent Microscopy: All the fluorescent images were taken with Nikon Eclipse Ti-E (Nikon, JP) equipped with a DS-Qi1 camera (Nikon, JP), a metal-halide fluorescence lamp (Nikon, JP) with a long-distance objective lens 40x (CFI S Plan Fluor ELWD, Nikon) and a fluorescent filter TRITC (543/593). The contrast and the brightness were adjusted and the image were presented with a false color for the figure.

Chemical Fixation: LNTs were chemically fixed as previously described[44]. The samples were incubated with osmium tetroxide (1% in 0.1 M cacodylate buffer solution, pH 7.4) and glutaraldehyde (2.5% in 0.1 M cacodylate buffer solution, pH 7.4) at 2:1 ratio at 0 °C for 30

min followed by rinse with HEPES buffer for three times. Then, the buffer solution was exchanged with ethanol gradually (15%, 30%, 50%, 75%, 80%, 95%, 100%) and finally exchanged with acetone. After the removal of acetone, the sample was completely dehydrated.

Electroless metal plating: A precursor aqueous solution of 29.4 mM chloroauric acid ($HAuCl_4$, #254169, Sigma-Aldrich, Switzerland) was prepared and stored under dark at 2 °C. A reducible plating solution was prepared by first heating the gold precursor solution (250 µL) to 60 °C and adding 0.5 µL H_2O_2 (Reactolab SA, Switzerland). The reducible plating solution (200 µL) was then added to the well with the fixed and dried AuNP coated LNTs. The samples were incubated at 70 °C while being shaken at 130 rpm for 5 min and immediately washed with water and subsequently with acetone. Over the course of the 5 min, the solution turned purple indicating the formation of Au nanostructures.

Transmission Electron Microscopy: Samples were prepared on 20, 50 or 200 nm-thick Si3N4 TEM membranes with 0.5 x 0.5 mm window (Plano GmbH, Germany) in a similar way to the one for glass substrates. Imaging was carried out with a FEI Tecnai G2 Sphera (FEI, Switzerland) operating at 120 kV acceleration voltage. The contrast was adjusted for the figures.

Scanning Electron Microscopy: Samples were prepared on silicon wafers in a similar way as on glass substrates. Imaging was carried out with a JEOL JSM-7600F (JEOL, Switzerland) in secondary electron imaging mode at energy levels of 5.0 kV and 20.0 kV at various magnifications. The contrast was adjusted for the figures. The instrument was equipped with an EDX detector with the model SDD X-MAX N80.

UV-VIS spectroscopy: Absorption spectra were obtained with V-670 (Jasco, USA). The samples deposited on glass coverslips were fixed with a hand-made sample holder. Absorption spectra were presented after removal of the background signal of clean glass coverslips.

Electrical Measurements: A cyclic voltammetry program with a two electrode setup was used to obtain I–V curves with an Autolab Potentiostat (Metrohm AG, Switzerland) equipped with Nova 2.1 software. Gold was sputtered on each side of the sample area by JEOL JFC-1200 Fine Coater (JEOL, Switzerland) for fabricating contact pads (roughly 5 mm in width and 2 mm distance between electrodes), which were connected to the potentiostat via crocodile connection.

RESULTS AND DISCUSSION

The schematic process for preparing AuNWs with self-assembled LNTs is shown in Figure 1A. The basic protocol for LNT surface assembly is described elsewhere.[44] In brief, first, DOPE, DOPE-Biotin and RhodaminePE were mixed in chloroform, dried, and rehydrated with HEPES buffer solution. Upon sonication, lipids form inverted hexagonal (H_{II}) blocks, which were attached to a glass coverslip functionalized with PLL-g-PEG-biotin-streptavidin. The PEG-coated area acts as a passivation surface to prevent nonspecific adsorption of AuNPs, while the exposed streptavidin on the surface is used to attach H_{II} lipid blocks through DOPE-Biotin. When a shear force created by a solution flow is applied to the lipid blocks, a part of the lipid blocks moves, while the other part remains adhered to the substrate, resulting in protruding LNTs. Next, to immobilize AuNPs along the LNTs, the formed LNTs were incubated in a streptavidin-coated AuNP solution. Figure 1BC show fluorescent images of self-assembled LNTs on glass substrates before (Figure 1B) and after (Figure 1C) attachment of 10 nm AuNPs. These images show that the addition of AuNPs does not disturb the LNT network,

although a slight change in the morphology was occasionally observed.

After coating the LNTs with AuNPs, they were chemically fixed, so that the LNTs withstand the following drying procedure. We used a combination of glutaraldehyde and osmium tetroxide, which are widely used in biology to prepare samples for electron microscopy.[52] After the fixation the amount of carbon double bonds (C=C) that were originally present in the tail of DOPE lipids decreased as seen by the reduction of the C=C peaks at 1695 cm^{-1} and 1639 cm^{-1} in the infrared spectra in Figure 1E. This suggests that osmium tetroxide reacted with them. This crosslinks the lipid tails, whereas one of the side products of this reaction is diolate species (reaction (b) in Figure 1D). This explains the broad peak that appeared after the fixation at 3340 cm^{-1} (OH), which is typical for free OH group. The peak at 1558 cm^{-1} (C-N) for dried lipids comes from the amine group in the DOPE headgroup. This group reacts with glutaraldehyde during fixation, which can be seen by the reduction of this peak after fixation. The peak at 3300 cm^{-1} (N-H) is also from the amine group, yet its overlap with the OH peak hinders the interpretation after fixation. This reaction forms imine groups between headgroups, which may be the peak that appeared at 1644 cm^{-1} (C=N) after fixation, although the overlap with the C=C peak makes it difficult to interpret. The peak at 1724 cm^{-1} (C=O) in dried lipids is due to the ester carbonyl groups in the head group of DOPE. After the fixation, an enhanced peak with a slight shift at 1735 cm^{-1} appeared. This is due to the C=O groups from glutaraldehyde that is either not reacted or reacted only on one side (reaction (a) in Figure 1D) overlapped in the same wavenumber region. The rest of the peaks are similar before and after fixation as expected. The assignment of the peaks is summarized in Table S1 in supplementary information.

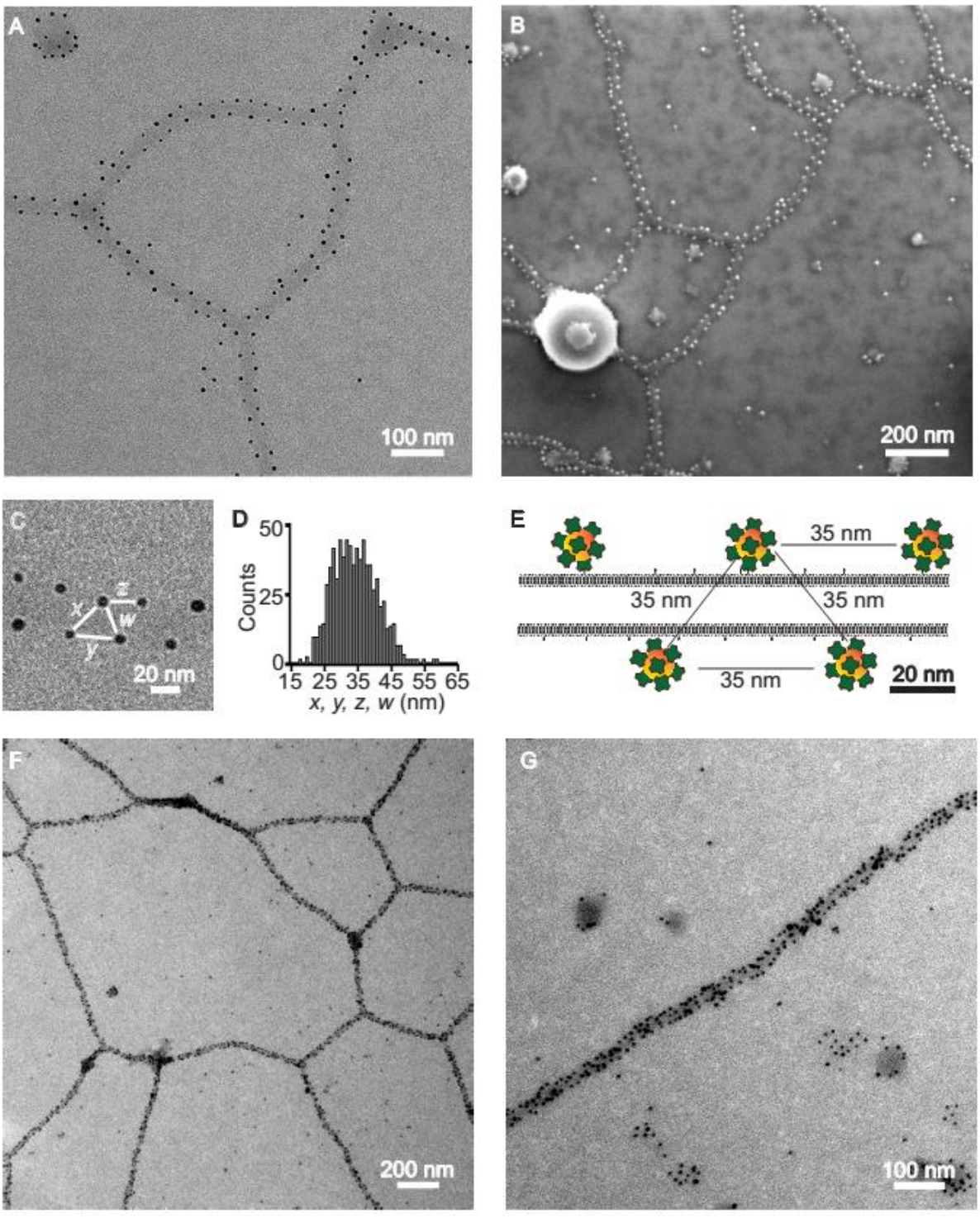

Figure 2: (A) Transmission electron microscopy and (B) scanning electron microscopy images of gold nanoparticle-attached lipid nanotubes at low nanoparticle concentration. (C, D, E) The distance between gold nanoparticles was equal at low concentration, which indicates inter-particle interactions. (F, G) Transmission electron microscopy images of gold nanoparticle-coated lipid nanotubes at high particle density.

This chemical fixation procedure cross-links both the head groups and the tails of the lipids, efficiently solidifying the LNTs without destroying the alignment of AuNPs. In our previous work,[44] we characterized the morphology of these AuNP-attached LNTs after fixation by atomic force microscopy (AFM). Although the resolution of AFM was sufficient to capture the presence of AuNPs, a lack of material contrast in this technique sometimes made it difficult to interpret the images. To overcome this issue, in this work, we characterized our samples with transmission electron microscopy (TEM) and scanning electron microscopy (SEM). Both techniques enable to distinguish materials by contrast in their images, because each element interacts with electrons in a different manner.

The background adsorption of AuNPs is successfully suppressed thanks to the PEG (Figure 2AB). Interestingly, both TEM (Figure 2A) and SEM (Figure 2B) visualized the alignment of AuNPs along the edge of the LNTs at low AuNP density. During the incubation, AuNPs should attach randomly onto the LNT surfaces. These obtained images suggest that after AuNPs are anchored to the LNTs they diffuse due to the fluidity of lipids until they find the substrate, where they adhere to the substrate via e.g. van der Waals interactions. This behavior is in agreement with the high lipid fluidity that has been previously characterized by fluorescence recovery after photobleaching (FRAP).[47-48] The distance between AuNPs, aligned along the edge of LNTs, is constant at 35 ± 10 nm (Figure 2C-E), which implies that there is a preferential distance between AuNPs due to the inter-particle interactions. This phenomenon took place only when we used the purchased streptavidin-coated AuNPs as it is, whereas it vanished when we centrifuged and resuspended in PBS buffer solution (Figure 2FG). The centrifugation and resuspension remove stabilizing agents such as glycerol (20%) and bovine serum albumin (BSA, 1%), and potentially free unbound streptavidin that may have been present in the solution. This suggests that the preferential distance is probably due to glycerol and BSA that

are known to add a shell to proteins[53-54] and to change the PEG conformation.[55] Note that the size distribution of the used AuNPs is reported as 10 nm.

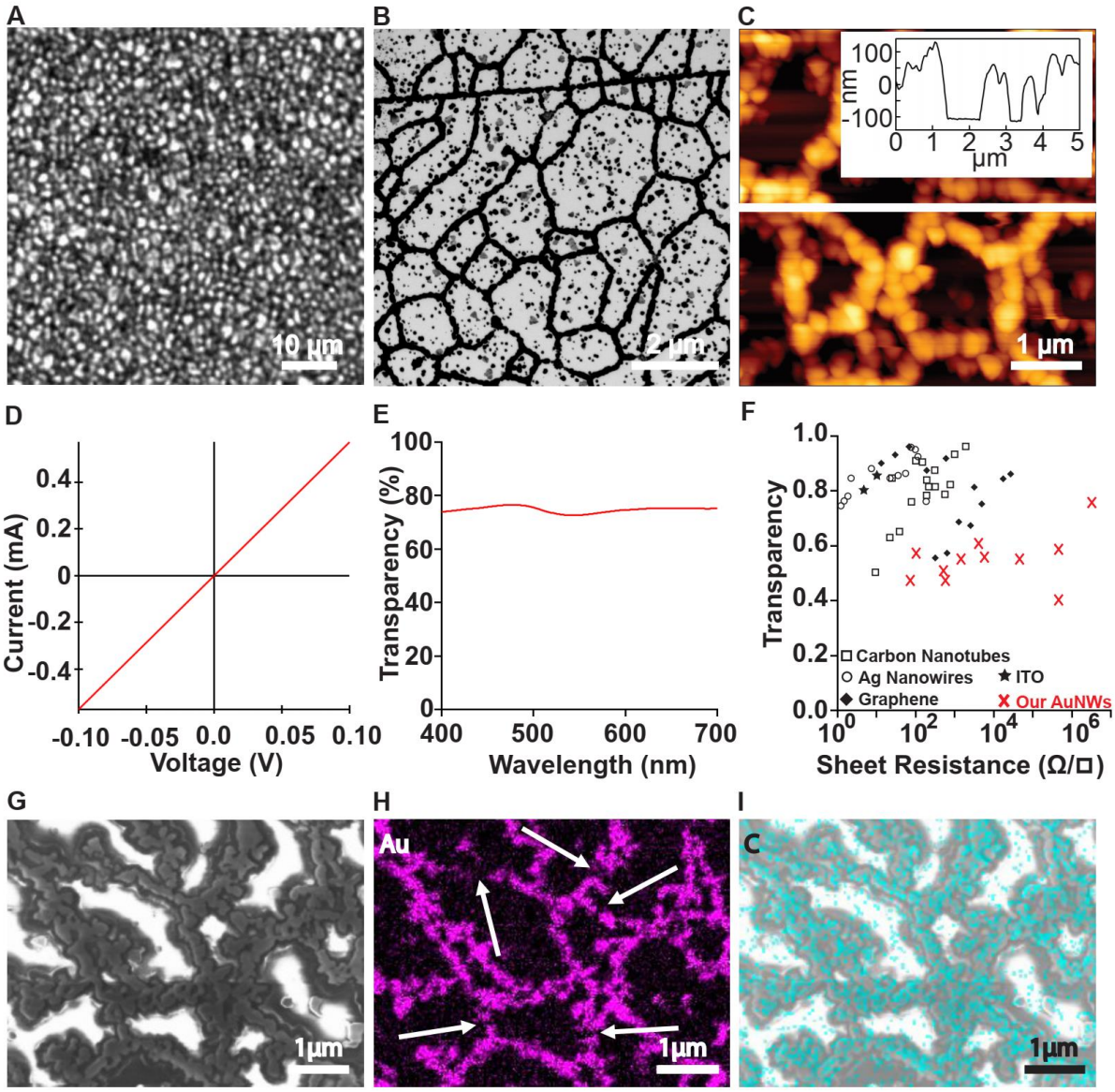

Figure 3: Representative (A) bright field, (B) scanning electron and (C) atomic force microscopy images of gold nanowires after electroless metal plating. (D) *I-V* curve for a sample and (E) its transparency profile. The typical surface plasmon resonance peaks from gold nanostructures can be seen at around 540 nm. (F) Electrical sheet resistance correlated with transparency for each sample, compared with the performance of other approaches in literature.[56-58] (G) SEM image of AuNWs, (H) corresponding EDX Au map and (I) EDX carbon map.

To improve the connection between these aligned AuNPs, we performed electroless metal plating on the surfaces (Figure 3A-C). Electroless metal plating[59-60] is a process, by which a metal is reduced onto a surface from its salt initially dissolved in the bulk without the need for an applied electrical potential. Here the aligned AuNPs were used as a catalyst for the plating reaction. The method used in this work is similar to the previously-reported technique for growing thin gold films on poly(vinyl pyrollidone) platinum loaded capsules.[61-62] After the optimization of the key parameters such as incubation time, temperature etc., the bright field (Figure 3A), SEM (Figure 3B), and AFM (Figure 3C) images all present the connection of AuNPs into wires. These Au nanowires did not form just with LNTs without attached AuNPs (Figure S1), suggesting the importance of the pre-aligned AuNPs as a catalyst. The Au salt solution stayed yellow during the plating, which implicates that the AuNPs that are larger than 5 nm (typically shows red color) did not form significantly in solution. This also supports that the metal plating is taking place on the substrate not in solution. The recipe for the metal plating is also important, as another reported method[63-65] failed to connect AuNPs due to the lack of fast and efficient metal growing on the substrate and the excess formation of additional AuNPs in solution (Figure S2). Neither pre-oxygen plasma treatment for removing the LNT template before plating (Figure S3AB) nor subsequent annealing after growing (Figure S3CD) were proven to be useful, because removing the template induces the instability in the alignment of AuNPs and the annealing tends to induce pearling of the nanowires due to the high surface tension of the liquid gold.[66-67] The fabricated substrates exhibited sheet resistance ranging 70 – 2000 Ω/□ (Figure 3DF), which is 11 orders of magnitude lower than our previous samples without electroless metal plating,[44] and transmission at 50-75% in visible wavelength (Figure 3EF). There is no strong correlation between the conductance and the transparency. This suggests that the variation in the conductance is due to the difference in the connectivity between gold nanoparticles at microscale. Energy-dispersive X-ray spectroscopy (EDX)

revealed disconnections of gold wires (see arrows in Figure 3H). The density of such a defect was roughly estimated as 2 disconnections per 5 μm which could explain the low conductivity of the sample. The transparency of the substrates can be explained by the gold surface coverage. AFM shows that the height of the gold wires is around 100 nm (Figure 3C). Control experiments suggest that a gold thin film above a thickness of 20 nm has almost no transmittance in visible light (Figure S7 in SI). Therefore, the transmittance from our substrates mainly originates from the glass region in between wires, which is around 50 % of the surface, matching with the transmittance (50-75%). To improve the transmittance, either the density or the height of the wires has to be reduced. Nevertheless, both reducing the wire density by adjusting the surface attachment of LNTs and the wire height by a shorter duration of metal plating would compromise the electrical conductance. If the samples are handled violently, the detachment of the Au mesh structure was occasionally observed (Figure S4), which also worsen the electrical connectivity. The performance of these samples is comparable to some of the reported graphene-based substrates (Figure 3F).[68-75] The advantage of our method is that we do not need an expensive instrument such as chemical or physical vapor deposition that other approaches (ITO, graphene, carbon nanotubes) would require. The material deposition can be more controlled and homogenous compared to Ag nanowires, which are typically spin-coated.[76-77]

CONCLUSION

We demonstrated the fabrication of transparent conductive films based on LNT templates that have fair transmittance (50-75%) because of the single layer metal mesh nanostructure and sheet resistance (70 – 2000 Ω/□) that is 11 orders of magnitude lower than our previous report[44] thanks to the electroless metal plating. These performances come from the improved

controllability of the nanowire deposition on substrates compared to spin-coating or embedding inside polymers that could suffer from lower or inhomogeneous transmittance due to the multilayer structures and lower conductance because of their poor connections. In contrast to other templating approaches that produce disconnected conductive nanoparticles such as metal plating of Tobacco mosaic virus[29-32] or DNA[33], our approach yields electrically-connected nanowire network over a macroscopic area. By replacing gold with other metal, a further reduction of the cost may be possible (see our preliminary efforts in Figure S5, S6 and Table S2 in SI). The molecular patterning approach based on LNT templates demonstrated in this work can be extrapolated towards biomolecule (e.g. protein) surface assembly[78] and even their patterning in an arbitrary shape for creating e.g. circuits by combining the previously-reported single LNT patterning technique with a micromanipulator.[47]

AUTHOR INFORMATION

Corresponding Author

*E-mail: kaori-s@iis.u-tokyo.ac.jp

Notes

The authors declare no competing financial interest.

ASSOCIATED CONTENT

Supplementary Information

Supporting Information for Table S1-S2 and Figure S1-S7 are available.

ACKNOWLEDGMENTS

Part of the research leading to these results has received funding from Swiss National Foundation, the Swiss National Centre of Competence in Research (NCCR) Chemical Biology, Fondation Ernst et Lucie Schmidheiny and Leading House for the Middle East and North Africa (University of Applied Sciences and Arts Western Switzerland). We thank Bioimaging center at the University of Geneva for access to TEM and SEM instruments and chemicals for fixation of samples, the CIME facility at EPFL for use of SEM instrument and Thomas Bürgi group for the use of UV-VIS spectrophotometer.

REFERENCES

(1) Gates, B. D.; Xu, Q. B.; Stewart, M.; Ryan, D.; Willson, C. G.; Whitesides, G. M., New Approaches to Nanofabrication: Molding, Printing, and Other Techniques. *Chemical Reviews* **2005**, *105*, 1171-1196.
(2) Hasan, R. M. M.; Luo, X., Promising Lithography Techniques for Next-Generation Logic Devices. *Nanomanufacturing and Metrology* **2018**, *1*, 67-81.
(3) Wang, Y. D.; Zhang, M. Y.; Lai, Y. K.; Chi, L. F., Advanced Colloidal Lithography: From Patterning to Applications. *Nano Today* **2018**, *22*, 36-61.
(4) Lohmuller, T., et al., Nano-Porous Electrode Systems by Colloidal Lithography for Sensitive Electrochemical Detection: Fabrication Technology and Properties. *Journal of Micromechanics and Microengineering* **2008**, *18*.
(5) Wang, Z. G.; Li, N.; Wang, T.; Ding, B. Q., Surface-Guided Chemical Processes on Self-Assembled DNA Nanostructures. *Langmuir* **2018**, *34*, 14954-14962.
(6) Schift, H., Nanoimprint Lithography: 2d or Not 2d? A Review. *Applied Physics a-Materials Science & Processing* **2015**, *121*, 415-435.
(7) Ivanisevic, A.; Mirkin, C. A., "Dip-Pen" Nanolithography on Semiconductor Surfaces. *Journal of the American Chemical Society* **2001**, *123*, 7887-7889.
(8) Husain, A. A. F.; Hasan, W. Z. W.; Shafie, S.; Hamidon, M. N.; Pandey, S. S., A Review of Transparent Solar Photovoltaic Technologies. *Renewable & Sustainable Energy Reviews* **2018**, *94*, 779-791.
(9) Sadasivuni, K. K.; Deshmukh, K.; Ahipa, T. N.; Muzaffar, A.; Ahamed, M. B.; Pasha, S. K. K.; Al-Maadeed, M. A., Flexible, Biodegradable and Recyclable Solar Cells: A Review. *Journal of Materials Science-Materials in Electronics* **2019**, *30*, 951-974.
(10) Werner, J. G.; Rodriguez-Calero, G. G.; Abruna, H. D.; Wiesner, U., Block Copolymer Derived 3-D Interpenetrating Multifunctional Gyroidal Nanohybrids for Electrical Energy Storage. *Energy & Environmental Science* **2018**, *11*, 1261-1270.

(11) Arthur, T. S.; Bates, D. J.; Cirigliano, N.; Johnson, D. C.; Malati, P.; Mosby, J. M.; Perre, E.; Rawls, M. T.; Prieto, A. L.; Dunn, B., Three-Dimensional Electrodes and Battery Architectures. *Mrs Bulletin* **2011**, *36*, 523-531.
(12) Tian, X. C.; Jin, J.; Yuan, S. Q.; Chua, C. K.; Tor, S. B.; Zhou, K., Emerging 3d-Printed Electrochemical Energy Storage Devices: A Critical Review. *Advanced Energy Materials* **2017**, *7*.
(13) Li, M.; Gou, H. L.; Al-Ogaidi, I.; Wu, N. Q., Nanostructured Sensors for Detection of Heavy Metals: A Review. *Acs Sustainable Chemistry & Engineering* **2013**, *1*, 713-723.
(14) Beluomini, M. A.; da Silva, J. L.; de Sa, A. C.; Buffon, E.; Pereira, T. C.; Stradiotto, N. R., Electrochemical Sensors Based on Molecularly Imprinted Polymer on Nanostructured Carbon Materials: A Review. *J. Electroanal. Chem.* **2019**, *840*, 343-366.
(15) Ahmad, O. S.; Bedwell, T. S.; Esen, C.; Garcia-Cruz, A.; Piletsky, S. A., Molecularly Imprinted Polymers in Electrochemical and Optical Sensors. *Trends in Biotechnology* **2019**, *37*, 294-309.
(16) Lazzara, T. D.; Mey, I.; Steinem, C.; Janshoff, A., Benefits and Limitations of Porous Substrates as Biosensors for Protein Adsorption. *Analytical Chemistry* **2011**, *83*, 5624-5630.
(17) Hokari, R.; Kurihara, K.; Higurashi, E.; Hiroshima, H., Optical Evaluation of Nanocomposite Metamaterials Fabricated by Nano-Printing Technique Utilizing Silver Nanoink. *Microelectron. Eng.* **2019**, *211*, 44-49.
(18) Zhang, C. Y.; Akbarzadeh, A.; Kang, W.; Wang, J. X.; Mirabolghasemi, A., Nano-Architected Metamaterials: Carbon Nanotube-Based Nanotrusses. *Carbon* **2018**, *131*, 38-46.
(19) Lee, J. H.; Singer, J. P.; Thomas, E. L., Micro-/Nanostructured Mechanical Metamaterials. *Advanced Materials* **2012**, *24*, 4782-4810.
(20) Fleming, S.; Stefani, A.; Tang, X. L.; Argyros, A.; Kemsley, D.; Cordi, J.; Lwin, R., Tunable Metamaterials Fabricated by Fiber Drawing. *Journal of the Optical Society of America B-Optical Physics* **2017**, *34*, D81-D85.
(21) Li, B. T.; Xiao, G.; Liu, F.; Qiao, Y.; Li, C. M.; Lu, Z. S., A Flexible Humidity Sensor Based on Silk Fabrics for Human Respiration Monitoring. *Journal of Materials Chemistry C* **2018**, *6*, 4549-4554.
(22) Park, J.; Lee, Y.; Ha, M.; Cho, S.; Ko, H., Micro/Nanostructured Surfaces for Self-Powered and Multifunctional Electronic Skins. *Journal of Materials Chemistry B* **2016**, *4*, 2999-3018.
(23) Ke, L.; Wang, Y. P.; Ye, X. X.; Luo, W.; Huang, X.; Shi, B., Collagen-Based Breathable, Humidity-Ultrastable and Degradable on-Skin Device. *Journal of Materials Chemistry C* **2019**, *7*, 2548-2556.
(24) Limongi, T.; Tirinato, L.; Pagliari, F.; Giugni, A.; Allione, M.; Perozziello, G.; Candeloro, P.; Di Fabrizio, E., Fabrication and Applications of Micro/Nanostructured Devices for Tissue Engineering. *Nano-Micro Letters* **2017**, *9*.
(25) Katana, B.; Rouster, P.; Varga, G.; Muráth, S.; Glinel, K.; Jonas, A. M.; Szilagyi, I., Self-Assembly of Protamine Biomacromolecule on Halloysite Nanotubes for Immobilization of Superoxide Dismutase Enzyme. *ACS Applied Bio Materials* **2020**, *3*, 522-530.
(26) Mi, G. J.; Shi, D.; Wang, M.; Webster, T. J., Reducing Bacterial Infections and Biofilm Formation Using Nanoparticles and Nanostructured Antibacterial Surfaces. *Advanced Healthcare Materials* **2018**, *7*.
(27) Tripathy, A.; Sen, P.; Su, B.; Briscoe, W. H., Natural and Bioinspired Nanostructured Bactericidal Surfaces. *Advances in Colloid and Interface Science* **2017**, *248*, 85-104.
(28) Jia, G.; Plentz, J.; Dellith, A.; Schmidt, C.; Dellith, J.; Schmidl, G.; Andrä, G., Biomimic Vein-Like Transparent Conducting Electrodes with Low Sheet Resistance and Metal Consumption. *Nano-Micro Letters* **2020**, *12*, 19.

(29) Rodriguez-Galvan, A.; Martinez-Loran, E.; Naveja, J. J.; Ornelas-Soto, N.; Basiuk, V. A.; Contreras-Torres, F. F., In-Situ Metallization of Thermally-Treated Tobacco Mosaic Virus Using Silver Nanoparticles. *Journal of Nanoscience and Nanotechnology* **2017**, *17*, 4740-4747.
(30) Zhou, J. C.; Soto, C. M.; Chen, M. S.; Bruckman, M. A.; Moore, M. H.; Barry, E.; Ratna, B. R.; Pehrsson, P. E.; Spies, B. R.; Confer, T. S., Biotemplating Rod-Like Viruses for the Synthesis of Copper Nanorods and Nanowires. *Journal of Nanobiotechnology* **2012**, *10*, 18.
(31) Bromley, K. M.; Patil, A. J.; Perriman, A. W.; Stubbs, G.; Mann, S., Preparation of High Quality Nanowires by Tobacco Mosaic Virus Templating of Gold Nanoparticles. *Journal of Materials Chemistry* **2008**, *18*, 4796-4801.
(32) Wnek, M.; Gorzny, M. L.; Ward, M. B.; Walti, C.; Davies, A. G.; Brydson, R.; Evans, S. D.; Stockley, P. G., Fabrication and Characterization of Gold Nano-Wires Templated on Virus-Like Arrays of Tobacco Mosaic Virus Coat Proteins. *Nanotechnology* **2013**, *24*, 025605.
(33) Bayrak, T.; Jagtap, N. S.; Erbe, A., Review of the Electrical Characterization of Metallic Nanowires on DNA Templates. *International Journal of Molecular Sciences* **2018**, *19*, 3019.
(34) Kinsella, J. M.; Ivanisevic, A., DNA-Templated Magnetic Nanowires with Different Compositions: Fabrication and Analysis. *Langmuir* **2007**, *23*, 3886-3890.
(35) Ijiro, K.; Mitomo, H., Metal Nanoarchitecture Fabrication Using DNA as a Biotemplate. *Polymer Journal* **2017**, *49*, 815-824.
(36) Richter, J.; Mertig, M.; Pompe, W.; Monch, I.; Schackert, H. K., Construction of Highly Conductive Nanowires on a DNA Template. *Applied Physics Letters* **2001**, *78*, 536-538.
(37) Geng, Y. L.; Pearson, A. C.; Gates, E. P.; Uprety, B.; Davis, R. C.; Harb, J. N.; Woolley, A. T., Electrically Conductive Gold- and Copper-Metallized DNA Origami Nanostructures. *Langmuir* **2013**, *29*, 3482-3490.
(38) Kim, H. J.; Roh, Y.; Hong, B., Selective Formation of a Latticed Nanostructure with the Precise Alignment of DNA-Templated Gold Nanowires. *Langmuir* **2010**, *26*, 18315-18319.
(39) Deng, Z. X.; Mao, C. D., DNA-Templated Fabrication of 1d Parallel and 2d Crossed Metallic Nanowire Arrays. *Nano Lett.* **2003**, *3*, 1545-1548.
(40) Yang, B.; Kamiya, S.; Shimizu, Y.; Koshizaki, N.; Shimizu, T., Glycolipid Nanotube Hollow Cylinders as Substrates: Fabrication of One-Dimensional Metallic-Organic Nanocomposites and Metal Nanowires. *Chemistry of Materials* **2004**, *16*, 2826-2831.
(41) Schnur, J. M., Lipid Tubules - a Paradigm for Molecularly Engineered Structures. *Science* **1993**, *262*, 1669-1676.
(42) Wagenbauer, K. F.; Sigl, C.; Dietz, H., Gigadalton-Scale Shape-Programmable DNA Assemblies. *Nature* **2017**, *552*, 78-83.
(43) Hui, L. W.; Zhang, Q. M.; Deng, W.; Liu, H. T., DNA-Based Nanofabrication: Pathway to Applications in Surface Engineering. *Small* **2019**, *15*.
(44) Jajcevic, K.; Chami, M.; Sugihara, K., Gold Nanowire Fabrication with Surface-Attached Lipid Nanotube Templates. *Small* **2016**, *12*, 4830-4836.
(45) Kozintsev, A.; Sugihara, K., Artificial Tubular Connections between Cells Based on Synthetic Lipid Nanotubes. *Rsc Advances* **2017**, *7*, 20700-20708.
(46) Sugihara, K., Self-Assembled Lipid Structures as Model Systems for Studying Electrical and Mechanical Properties of Cell Membranes. *Chimia* **2016**, *70*, 805-809.
(47) Sugihara, K.; Rustom, A.; Spatz, J. P., Freely Drawn Single Lipid Nanotube Patterns. *Soft Matter* **2015**, *11*, 2029-2035.
(48) Sugihara, K.; Chami, M.; Derenyi, I.; Voros, J.; Zambelli, T., Directed Self-Assembly of Lipid Nanotubes from Inverted Hexagonal Structures. *Acs Nano* **2012**, *6*, 6626-6632.
(49) Sugihara, K.; Delai, M.; Mahnna, R.; Kusch, J.; Poulikakos, D.; Voros, J.; Zambelli, T.; Ferrari, A., Label-Free Detection of Cell-Contractile Activity with Lipid Nanotubes. *Integrative Biology* **2013**, *5*, 423-430.

(50) Chang, D. P.; Jankunec, M.; Barauskas, J.; Tiberg, F.; Nylander, T., Adsorption of Lipid Liquid Crystalline Nanoparticles: Effects of Particle Composition, Internal Structure, and Phase Behavior. *Langmuir* **2012**, *28*, 10688-10696.
(51) Tabaei, S. R.; Choi, J. H.; Zan, G. H.; Zhdanov, V. P.; Cho, N. J., Solvent-Assisted Lipid Bilayer Formation on Silicon Dioxide and Gold. *Langmuir* **2014**, *30*, 10363-10373.
(52) Eltoum, I.; Fredenburgh, J.; Myers, R. B.; Grizzle, W. E., Introduction to the Theory and Practice of Fixation of Tissues. *Journal of Histotechnology* **2001**, *24*, 173-190.
(53) Hansen, J.; Platten, F.; Wagner, D.; Egelhaaf, S. U., Tuning Protein-Protein Interactions Using Cosolvents: Specific Effects of Ionic and Non-Ionic Additives on Protein Phase Behavior. *Physical Chemistry Chemical Physics* **2016**, *18*, 10270-10280.
(54) Vagenende, V.; Yap, M. G. S.; Trout, B. L., Mechanisms of Protein Stabilization and Prevention of Protein Aggregation by Glycerol. *Biochemistry* **2009**, *48*, 11084-11096.
(55) Leopold, L. F.; Todor, I. S.; Diaconeasa, Z.; Rugina, D.; Stefancu, A.; Leopold, N.; Coman, C., Assessment of Peg and Bsa-Peg Gold Nanoparticles Cellular Interaction. *Colloids and Surfaces a-Physicochemical and Engineering Aspects* **2017**, *532*, 70-76.
(56) Sharma, S.; Shriwastava, S.; Kumar, S.; Bhatt, K.; Tripathi, C. C., Alternative Transparent Conducting Electrode Materials for Flexible Optoelectronic Devices. *Opto-Electronics Review* **2018**, *26*, 223-235.
(57) Cao, W. R.; Li, J.; Chen, H. Z.; Xue, J. G., Transparent Electrodes for Organic Optoelectronic Devices: A Review. *Journal of Photonics for Energy* **2014**, *4*, 040990.
(58) Naghdi, S.; Rhee, K. Y.; Hui, D.; Park, S. J., A Review of Conductive Metal Nanomaterials as Conductive, Transparent, and Flexible Coatings, Thin Films, and Conductive Fillers: Different Deposition Methods and Applications. *Coatings* **2018**, *8*, 278.
(59) Lahiri, A.; Kobayashi, S. I., Electroless Deposition of Gold on Silicon and Its Potential Applications: Review. *Surf. Eng.* **2016**, *32*, 321-337.
(60) Shacham-Diamand, Y.; Osaka, T.; Okinaka, Y.; Sugiyama, A.; Dubin, V., 30 Years of Electroless Plating for Semiconductor and Polymer Micro-Systems. *Microelectron. Eng.* **2015**, *132*, 35-45.
(61) Hitchcock, J. P.; Tasker, A. L.; Baxter, E. A.; Biggs, S.; Cayre, O. J., Long-Term Retention of Small, Volatile Molecular Species within Metallic Microcapsules. *Acs Applied Materials & Interfaces* **2015**, *7*, 14808-14815.
(62) Tasker, A. L.; Hitchcock, J.; Baxter, E. A.; Cayre, O. J.; Biggs, S., Understanding the Mechanisms of Gold Shell Growth onto Polymer Microcapsules to Control Shell Thickness. *Chemistry-an Asian Journal* **2017**, *12*, 1641-1648.
(63) Brinson, B. E.; Lassiter, J. B.; Levin, C. S.; Bardhan, R.; Mirin, N.; Halas, N. J., Nanoshells Made Easy: Improving Au Layer Growth on Nanoparticle Surfaces. *Langmuir* **2008**, *24*, 14166-14171.
(64) Lin, N.; Zhang, W. X.; Koshel, B. M.; Cheng, J. X.; Yang, C., Spatially Modulated Two-Photon Luminescence from Si-Au Core-Shell Nanowires. *Journal of Physical Chemistry C* **2011**, *115*, 3198-3202.
(65) Mandal, S.; Shundo, A.; Acharya, S.; Hill, J. P.; Ji, Q. M.; Ariga, K., Hydrogen-Bond-Assisted "Gold Cold Fusion" for Fabrication of 2d Web Structures. *Chemistry-an Asian Journal* **2009**, *4*, 1055-1058.
(66) Karim, S.; Toimil-Molares, M. E.; Balogh, A. G.; Ensinger, W.; Cornelius, T. W.; Khan, E. U.; Neumann, R., Morphological Evolution of Au Nanowires Controlled by Rayleigh Instability. *Nanotechnology* **2006**, *17*, 5954-5959.
(67) Vigonski, S.; Jansson, V.; Vlassov, S.; Polyakov, B.; Baibuz, E.; Oras, S.; Aabloo, A.; Djurabekova, F.; Zadin, V., Au Nanowire Junction Breakup through Surface Atom Diffusion. *Nanotechnology* **2018**, *29*, 015704.

(68) Liu, C. H.; Yu, X., Silver Nanowire-Based Transparent, Flexible, and Conductive Thin Film. *Nanoscale Research Letters* **2011**, *6*, 75.
(69) Vinogradov, V. V.; Agafonov, A.; Avnir, D., Conductive Sol-Gel Films. *Journal of Materials Chemistry C* **2014**, *2*, 3914-3920.
(70) Kim, W. K., et al., Cu Mesh for Flexible Transparent Conductive Electrodes. *Scientific Reports* **2015**, *5*, 10715.
(71) Morag, A.; Jelinek, R., "Bottom-up" Transparent Electrodes. *Journal of Colloid and Interface Science* **2016**, *482*, 267-289.
(72) Kamyshny, A.; Magdassi, S., Conductive Nanomaterials for Printed Electronics. *Small* **2014**, *10*, 3515-3535.
(73) Xue, J.; Song, J. Z.; Dong, Y. H.; Xu, L. M.; Li, J. H.; Zeng, H. B., Nanowire-Based Transparent Conductors for Flexible Electronics and Optoelectronics. *Science Bulletin* **2017**, *62*, 143-156.
(74) Shin, K.; Park, J. S.; Han, J. H.; Choi, Y.; Chung, D. S.; Kim, S. H., Patterned Transparent Electrode with a Continuous Distribution of Silver Nanowires Produced by an Etching-Free Patterning Method. *Scientific Reports* **2017**, *7*, 40087.
(75) Mohl, M.; Dombovari, A.; Vajtai, R.; Ajayan, P. M.; Kordas, K., Self-Assembled Large Scale Metal Alloy Grid Patterns as Flexible Transparent Conductive Layers. *Scientific Reports* **2015**, *5*, 13710.
(76) Wang, H.; Wang, Y.; Chen, X. M., Synthesis of Uniform Silver Nanowires from Agcl Seeds for Transparent Conductive Films Via Spin-Coating at Variable Spin-Speed. *Colloids and Surfaces a-Physicochemical and Engineering Aspects* **2019**, *565*, 154-161.
(77) Langley, D.; Giusti, G.; Mayousse, C.; Celle, C.; Bellet, D.; Simonato, J. P., Flexible Transparent Conductive Materials Based on Silver Nanowire Networks: A Review. *Nanotechnology* **2013**, *24*, 452001.
(78) Shimizu, T., Self-Assembly of Discrete Organic Nanotubes. *Bulletin of the Chemical Society of Japan* **2018**, *91*, 623-668.

TOC GRAPHIC

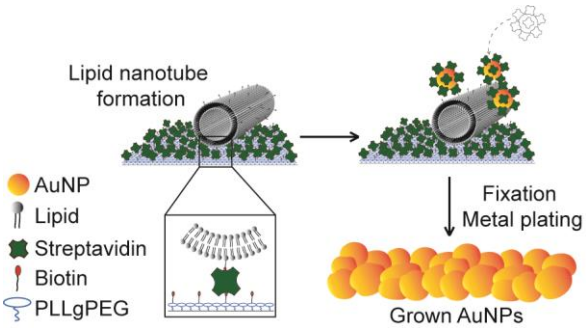
Lipid nanotube
formation
AuNP
Lipid
Streptavidin
Biotin
PLLgPEG
Fixation
Metal plating
Grown AuNPs